American Mineralogist, Volume 86, pages 566–577, 2001

Displacive components of the low-temperature phase transitions in lawsonite

HINRICH-WILHELM MEYER,[1,*] STEFAN MARION,[2] PETER SONDERGELD,[3] MICHAEL A. CARPENTER,[1] KEVIN S. KNIGHT,[4] SIMON A.T. REDFERN,[1] AND MARTIN T. DOVE[1]

[1]Department of Earth Sciences, University of Cambridge, Downing Street, Cambridge CB2 3EQ, U.K.
[2]University of Oslo, Center for Materials Science, N-0349 Oslo, Norway
[3]Institut für Experimentalphysik, Universität Wien, Strudlhofgasse 4, A-1090 Wien, Austria
[4]ISIS Facility, Rutherford Appleton Laboratory, Chilton, Didcot, Oxfordshire, OX11 OQX, U.K.

ABSTRACT

The phase transitions in deuterated lawsonite were investigated with high-resolution, time-of-flight neutron diffraction between 2 and 500 K. From the analysis of spontaneous strain data, the thermodynamics of the phase transition at 273 K are not changed by the deuteration process. Shifts in atomic positions with temperature indicate continuous changes for a framework oxygen and for one of the deuterium atoms, whereas for the other deuterium atom, a more discontinuous behavior was observed in the average structure. Comparison of O···D and O···O bond lengths with IR data from a non-deuterated lawsonite permits a detailed analysis of assignments of O-H stretching modes.

INTRODUCTION

Lawsonite has attracted considerable interest over the last few years both because of its importance as a marker of moderate *P* and low *T* conditions in nature (Pawley 1994; Pawley et al. 1996; Schmidt 1995) and because it exhibits phase transitions arising from interactions between hydrogen bonding and lattice relaxations (Libowitzky and Armbruster 1995; Libowitzky and Rossman 1996; Lager et al. 1999; Meyer et al. 2000; Sondergeld et al. 2000; Martin-Olalla et al. 2001). Libowitzky and Armbruster (1995) reported two phase transitions, one at 273 ± 5 K, and the second below 155 K. They described the room-temperature transition in terms of the development of co-operative hydrogen bonds. The aim of the present powder neutron diffraction study was to address the following questions: (1) Does the exchange of deuterium for hydrogen change the critical temperatures and the thermodynamic character of the transitions? (2) How do the positions of the deuterium atoms evolve with temperature and how does their behavior correlate with the results from X-ray structure determinations and IR experiments? (3) Is it possible to clarify details of the mechanism of the transition at 273 K in terms of the contributions of proton ordering and framework displacements? The data collected also allow some further analysis of the relationships between bond lengths and vibrational frequencies for hydrogen bonding.

METHODS

The lawsonite sample is from Valley Ford, Sonoma County, California (sample no. 120943 of the Harvard mineral collection). A sample from this batch was studied by Meyer et al. (2000). The composition of the sample was determined by electron microprobe analysis (EMPA) on a Cameca Camebax instrument, operating at 20 kV and 3 nA. Elements with concentrations less than 2σ were excluded from further consideration, and consequently only Ca, Al, Fe and Si were taken into account. The average of four analyses, based on eight oxygen atoms per atomic formula unit, is Ca 1.00, Al 1.95, Fe 0.05, Si 2.01, where the estimated uncertainties are ±0.01.

To provide a deuterated sample suitable for neutron diffraction, powdered lawsonite with an average grain size of ~77 μm was separated using heavy liquids. Approximately 1 g of this powder was placed in a platinum sample holder, which was mounted in a closed, gas-tight furnace (details in Marion et al., in preparation). The deuteration was achieved by flowing dried Ar gas at room temperature through a bottle of D_2O and subsequently through the hot zone of the furnace, where the exchange reaction took place. The experiments were performed at 425 °C at a vapor pressure of approximately 3.2 kPa. The progress of the deuteration reaction was followed via a thermo-balance. From static proton NMR spectroscopy experiments the sample was 90.5 ± 2.5% deuterated.

Neutron powder diffraction data were collected using the time-of-flight high-resolution diffractometer HRPD (Johnson and David 1985, Ibberson et al. 1992) at the ISIS neutron spallation source (Rutherford Appleton Laboratory). For the experiments, 3 grams of deuterated lawsonite were packed in an aluminum can with thin vanadium front and back windows. This and a 100 W cartridge heater were then mounted on a candlestick sample holder. The complete sample set-up was subsequently quenched in liquid nitrogen before being introduced into a helium cryo-furnace, where it was cooled to 2 K. During cooling from 100 K the diffraction pattern was constantly monitored for any signs of unwanted effects. None were observed. The data sets were focused to a Bragg angle of 168.329° and normalized to the incident monitor spectrum. The background was subtracted and the data were corrected for detector efficiency using a diffraction pattern from vanadium.

* E-mail: hmeyer@esc.cam.ac.uk

All data sets were collected from 32000 μs to 230000 μs in time channel bins of $\Delta t/t = 1 \times 10^{-4}$, the time window corresponding to a *d*-spacing of 0.66 to 2.49 Å in the back-scattering detector bank. The following data collection times were employed: 200 μAh for the data set at 2 K, 180 μAh for the data sets between 50 K and 285 K, and 100 μAh for data sets collected at 300, 350 and 400 K. The data set at 500 K was collected for about 45 minutes before the end of the allocated experiment time. All data collections included a 15 minute interval at each temperature prior to data collection to allow for thermal equilibration.

Rietveld refinements were carried out using the program GSAS (Larson and Von Dreele 1994). Starting values for lattice parameters and atomic positions were taken from Libowitzky and Armbruster (1995). The data set at 500 K was sufficient for the refinement of lattice parameters only, but at all other temperatures, full structure refinements were performed. The data sets were refined with isotropic atomic displacement factors and convergence was rapidly achieved. Refinement results of the atomic displacement factors for the Al positions were non-positive and so estimates of the occupancies for this site were derived from bond-length calculations. A small amount of Fe^{3+} (3% of the site occupancy of Al) was introduced and gave reasonable results for the displacement parameters of the octahedral site. This amount is in good agreement with the electron microprobe analysis. Refinement with anisotropic atomic displacement parameters and split-sites for the deuterium positions did not result in crystallographically meaningful values. Details of the refinement parameters are in Table 1, the refined lattice parameters are in Table 2, and refined atomic positions and isotropic atomic displacement parameters are in Table 3. The variations of lattice parameters with temperature are shown in Figure 1.

TABLE 1. Refinement details for all temperatures

T (K)	space group	parameters refined	χ^2	*wR*p	*R*p
2	$P2_1cn$	84	3.232	0.0556	0.0540
50	$P2_1cn$	84	3.688	0.0388	0.0365
100	$P2_1cn$	84	3.435	0.0585	0.0552
130	*Pmcn*	61	3.475	0.0626	0.0588
175	*Pmcn*	61	4.348	0.0664	0.0619
225	*Pmcn*	61	4.278	0.0656	0.0604
268	*Pmcn*	61	5.981	0.0780	0.0690
285	*Cmcm*	42	8.468	0.0941	0.0796
300	*Cmcm*	42	4.787	0.0971	0.0845
350	*Cmcm*	42	4.074	0.0948	0.0833
400	*Cmcm*	42	3.848	0.0910	0.0797
500	*Cmcm*	42	1.457	0.1619	0.1438

RESULTS

Strain analysis

To check if the H-D exchange had actually changed the thermodynamic character of the transitions, spontaneous strains were calculated from the refined lattice parameters. These were compared to spontaneous strain data from non-deuterated samples (from Meyer et al. 2000). The spontaneous strains were calculated in the manner described by Carpenter et al. (1998) using the following formulae for lattice constants and the unit cell volume:

$$e_1 = \frac{a - a_0}{a_0},\ e_2 = \frac{b - b_0}{b_0},\ e_3 = \frac{c - c_0}{c_0},\ \text{and}\ e_{\text{vol}} = \frac{V - V_0}{V_0} \qquad (1)$$

The baseline used to calculate the values of a_0, b_0, c_0, and V_0 was taken from Meyer et al. (2000). It is of the form $y = y_c + y_1 \cdot \theta_s \cdot \coth(\theta_s/T)$ and describes plateau-like features in the lattice constants and the unit-cell volume (Fig. 1) at low temperatures and a linear behavior at high temperatures. θ_s is a material constant and is related to the temperature at which the temperature dependence changes from constant to linear (Salje et al. 1991a, 1991b).

The results of the strain calculations are compared in Figure 2 with spontaneous strain data from X-ray powder diffraction and dilatometry experiments [taken from Meyer et al. (2000)]. In all three crystallographic directions, the strains from neutron diffraction qualitatively describe the same effects as the strains from other experiments. The strains are small and differences in the data relate to both the limited resolution of the X-ray equipment and to uncertainties in defining the baseline in each experiment. The experimental uncertainty in the neutron data propagated from the estimated standard deviation values for the lattice parameters is ~0.01%, but the real uncertainty is probably somewhat greater.

The square of the strains, e_i^2 in Figure 3, show a linear dependency below the transition temperature of 273 K (T_1), which indicates that the transition is being tricritical in character ($Q^4 \propto |T_c - T|$). A linear fit to the data gives a critical temperature of 273 K for e_1, which is in excellent agreement with the result from heat capacity measurements (Martin-Olalla et al. 2001). The heat capacity measurements also indicated a tricritical behavior for the transition at T_1 (Martin-Olalla et al. 2001). There are insufficient data for a precise determination of the critical temperature or a strain analysis for the second transition at T_2 (<155 K).

Atomic positions

In Figure 4 Fourier maps, based on observed structure factors, are displayed for sections parallel to (100) at temperatures between 2 and 400 K. All maps show an equivalent part of the structure which contains a sequence of D_2O-OD-OD-D_2O highly affected by the temperature changes. An equivalent part of the structure is shown as a polyhedral drawing in Figure 5. Figure 4, lower right, shows the high-symmetry structure at 400 K. Mirror planes, which relate the two deuterium atoms of the D_2O molecule to each other, are shown by dashed lines. On cooling through the first phase transition at $T_1 = 273$ K this mirror-plane is lost and the D_2O molecule starts to rotate in the plane of the map. This effect increases on further cooling (center of Fig. 4). On further cooling, a second mirror-plane perpendicular to the first is lost and the Dwa atom leaves its place and moves out of the plane to give rise to the previously observed ferroelectric pattern (Sondergeld et al. 2000). The maps in Figure 6, which are sections perpendicular to the maps in Figure 4 through the D_2O-OD-OD-D_2O chains, show the violations of the second mirror plane at 2 K and 100 K. The orientation of these sections is perpendicular to (100) and along the

TABLE 2. Refined lattice parameters of lawsonite between 2 and 500 K

T (K)	*a* (Å)	*b* (Å)	*c* (Å)	*V* (Å^3)
2	5.86465(2)	8.7652(3)	13.1002(5)	673.413(3)
50	5.8639(2)	8.76442(4)	13.099(5)	673.208(3)
100	5.86332(2)	8.76659(4)	13.1021(5)	673.464(3)
130	5.86243(2)	8.76981(4)	13.1063(5)	673.825(3)
175	5.86092(2)	8.77586(4)	13.1132(6)	674.473(3)
225	5.85942(2)	8.78269(4)	13.1209(6)	675.223(4)
268	5.85539(3)	8.79152(5)	13.1326(7)	676.036(4)
285	5.85424(3)	8.79471(6)	13.1365(8)	676.350(5)
300	5.8543(4)	8.79679(7)	13.1387(9)	676.628(6)
350	5.85603(3)	8.80228(7)	13.1442(9)	677.533(6)
400	5.85851(3)	8.80727(7)	13.149(8)	678.457(5)
500	5.8642(5)	8.817(1)	13.159(1)	680.415(9)

TABLE 3a. Atomic positional parameters of lawsonite in space group $P2_1cn$ at 2, 50, and 100 K

Atom	*T* (K)	*x*	*y*	*z*	U_{iso}*100 (Å^2)
Ca	2	–0.266(3)	0.0812(3)	0.2511(3)	0.35(8)
	50	–0.272(3)	0.0811(3)	0.2506(3)	0.26(8)
	100	–0.269(3)	0.0813(3)	0.2503(4)	0.33(9)
Al	2	0	–0.000(2)	–0.002(1)	0.15(5)
	50	0	0.000(2)	–0.004(1)	0.13(6)
	100	0	0.000(2)	–0.004(1)	0.17(5)
Ala	2	0.002(3)	–0.002(2)	0.498(1)	0.15(5)
	50	–0.006(4)	–0.002(2)	0.497(1)	0.13(6)
	100	0.005(4)	–0.002(2)	0.505(1)	0.17(5)
Si	2	–0.248(3)	0.731(5)	0.133(3)	0.21(4)
	50	–0.253(4)	0.730(5)	0.132(4)	0.11(5)
	100	–0.252(4)	0.730(5)	0.132(4)	0.18(5)
Sia	2	–0.250(3)	0.727(5)	0.366(3)	0.21(4)
	50	–0.254(4)	0.727(5)	0.366(4)	0.11(5)
	100	–0.249(4)	0.727(5)	0.366(4)	0.18(5)
O1	2	–0.239(2)	–0.2016(2)	0.2485(3)	0.30(5)
	50	–0.247(3)	–0.2016(3)	0.2485(3)	0.44(6)
	100	–0.244(3)	–0.20172(3)	0.2485(3)	0.46(6)
O2	2	0.024(2)	0.1185(8)	0.1250(5)	0.27(3)
	50	0.017(3)	0.1185(8)	0.1248(5)	0.28(3)
	100	0.018(3)	0.1184(9)	0.1218(6)	0.37(3)
O2a	2	0.021(3)	0.1261(8)	0.3819(5)	0.27(3)
	50	0.013(3)	0.1255(9)	0.3819(5)	0.28(3)
	100	0.015(3)	0.127(1)	0.3862(6)	0.37(3)
O2b	2	0.474(3)	0.3674(8)	0.8870(5)	0.27(3)
	50	0.466(3)	0.3664(8)	0.8869(5)	0.28(3)
	100	0.467(3)	0.3675(9)	0.8824(6)	0.37(3)
O2c	2	0.475(2)	0.3740(8)	0.6170(5)	0.27(3)
	50	0.468(2)	0.3741(9)	0.6170(5)	0.28(3)
	100	0.470(3)	0.374(1)	0.6197(6)	0.37(3)
O3	2	–0.253(3)	–0.1130(4)	0.0636(2)	0.15(3)
	50	–0.261(3)	–0.1132(4)	0.0635(3)	0.14(4)
	100	–0.257(3)	–0.1135(4)	0.0637(3)	0.16(4)
O3a	2	–0.252(3)	–0.1155(4)	0.4339(2)	0.15(3)
	50	–0.257(3)	–0.1154(4)	0.4337(2)	0.14(4)
	100	–0.256(3)	–0.1147(4)	0.4341(2)	0.16(4)
O4	2	–0.258(3)	0.3916(4)	0.0513(2)	0.16(4)
	50	–0.264(3)	0.3912(4)	0.0512(2)	0.22(4)
	100	–0.263(3)	0.3919(4)	0.0513(2)	0.26(4)
O4a	2	–0.247(3)	0.3806(4)	0.4613(2)	0.16(4)
	50	–0.255(3)	0.3806(4)	0.4609(2)	0.22(4)
	100	–0.255(3)	0.3806(4)	0.4609(2)	0.26(4)
O5	2	–0.234(2)	0.3589(3)	0.2479(3)	0.41(7)
	50	–0.239(3)	0.3592(3)	0.2482(4)	0.39(7)
	100	–0.241(3)	0.3590(4)	0.2485(4)	0.72(7)
Dw	2	–0.250(3)	0.3826(4)	0.1721(3)	2.26(7)
	50	–0.259(3)	0.3827(5)	0.1726(3)	2.26(8)
	100	–0.260(3)	0.3842(5)	0.1726(3)	2.43(9)
Dwa	2	0.699(2)	0.4402(5)	0.2841(3)	3.5(1)
	50	0.694(3)	0.4408(5)	0.2843(3)	3.2(1)
	100	0.701(3)	0.4410(5)	0.2851(3)	3.6(1)
Dh	2	–0.250(3)	0.2797(4)	0.0290(2)	1.93(7)
	50	–0.256(3)	0.2792(4)	0.0288(3)	2.17(9)
	100	–0.254(3)	0.2797(4)	0.0295(3)	2.16(8)
Dha	2	–0.234(3)	0.3227(4)	0.4014(3)	2.8(1)
	50	–0.243(3)	0.3225(4)	0.4017(3)	2.9(1)
	100	–0.240(3)	0.3218(4)	0.4024(3)	3.0(1)

TABLE 3b. Atomic positional parameters of lawsonite in space group *Pmcn* at 130, 175, 225 and 268 K

Atom	*T* (K)	*x*	*y*	*z*	U_{iso}*100 (Å^2)
Ca	130	–1/4	0.0812(3)	0.2496(4)	0.59(6)
	175	–1/4	0.0810(4)	0.2493(4)	0.65(7)
	225	–1/4	0.0812(4)	0.2492(5)	0.83(7)
	268	–1/4	0.0803(5)	0.2471(7)	0.92(9)
Al	130	0	0	0	0.10(5)
	175	0	0	0	0.16(6)
	225	0	0	0	0.26(6)
	268	0	0	0	0.40(8)
Ala	130	0	0	1/2	0.10(5)
	175	0	0	1/2	0.16(6)
	225	0	0	1/2	0.26(6)
	268	0	0	1/2	0.40(8)
Si	130	–1/4	0.7298(6)	0.1319(4)	0.29(5)
	175	–1/4	0.7291(7)	0.1324(4)	0.38(5)
	225	–1/4	0.7298(7)	0.1323(4)	0.39(6)
	268	–1/4	0.731(1)	0.1312(6)	0.37(7)
Sia	130	–1/4	0.7285(6)	0.3659(4)	0.29(5)
	175	–1/4	0.7292(7)	0.3664(4)	0.38(5)
	225	–1/4	0.7291(7)	0.3660(5)	0.39(6)
	268	–1/4	0.729(1)	0.3664(6)	0.37(7)
O1	130	–1/4	-0.2019(3)	0.2487(3)	0.42(5)
	175	–1/4	-0.2020(3)	0.2488(4)	0.57(6)
	225	–1/4	-0.2022(3)	0.2492(4)	0.61(6)
	268	–1/4	-0.2034(4)	0.2510(6)	0.68(8)
O2	130	0.0243(5)	0.1226(3)	0.1207(2)	0.40(3)
	175	0.0235(6)	0.1231(3)	0.1202(2)	0.45(3)
	225	0.0224(7)	0.1242(4)	0.1195(2)	0.49(3)
	268	0.021(1)	0.1270(6)	0.1179(3)	0.50(4)
O2a	130	0.0230(5)	0.1230(3)	0.3848(2)	0.40(3)
	175	0.0230(6)	0.1305(3)	0.3847(2)	0.45(3)
	225	0.0234(7)	0.1304(4)	0.3845(2)	0.49(3)
	268	0.024(1)	0.1289(5)	0.3842(3)	0.50(4)
O3	130	–1/4	-0.1139(4)	0.0628(3)	0.23(4)
	175	–1/4	-0.1137(5)	0.0636(3)	0.27(4)
	225	–1/4	-0.1138(5)	0.0638(3)	0.39(4)
	268	–1/4	-0.1135(8)	0.0661(4)	0.34(5)
O3a	130	–1/4	-0.1136(4)	0.4333(2)	0.23(4)
	175	–1/4	-0.1137(5)	0.4332(3)	0.27(4)
	225	–1/4	-0.1129(5)	0.4330(3)	0.39(4)
	268	–1/4	-0.1116(8)	0.4333(4)	0.34(5)
O4	130	–1/4	0.3925(4)	0.0514(2)	0.29(4)
	175	–1/4	0.3934(5)	0.0512(3)	0.44(5)
	225	–1/4	0.3943(5)	0.0515(3)	0.49(5)
	268	–1/4	0.3936(8)	0.0516(5)	0.76(6)
O4a	130	–1/4	0.3812(4)	0.4612(3)	0.29(4)
	175	–1/4	0.3822(5)	0.4601(3)	0.44(5)
	225	–1/4	0.3835(5)	0.4594(3)	0.49(5)
	268	–1/4	0.3868(8)	0.4577(4)	0.76(6)
O5	130	–1/4	0.3575(4)	0.2482(4)	1.21(6)
	175	–1/4	0.3580(4)	0.2484(5)	1.42(7)
	225	–1/4	0.3586(4)	0.2488(5)	1.83(8)
	268	–1/4	0.3599(6)	0.249(1)	2.2(1)
Dw	130	–1/4	0.3841(5)	0.1723(3)	2.80(9)
	175	–1/4	0.3875(6)	0.1734(4)	3.2(1)
	225	–1/4	0.3912(6)	0.1746(4)	3.8(1)
	268	–1/4	0.407(1)	0.1805(8)	5.7(3)
Dwa	130	–1/4	0.4379(6)	0.2878(4)	5.9(1)
	175	–1/4	0.4371(7)	0.2902(4)	5.8(2)
	225	–1/4	0.4337(7)	0.2925(4)	6.0(2)
	268	–1/4	0.420(1)	0.3015(8)	6.4(3)
Dd	130	–1/4	0.2797(4)	0.0313(3)	2.13(8)
	175	–1/4	0.2796(5)	0.0329(3)	2.38(9)
	225	–1/4	0.2794(5)	0.0350(3)	2.6(1)
	268	–1/4	0.2781(7)	0.0383(5)	3.6(2)
Dda	130	–1/4	0.3189(5)	0.4042(3)	3.1(1)
	175	–1/4	0.3158(6)	0.4063(4)	3.8(1)
	225	–1/4	0.3132(6)	0.4092(4)	4.3(1)
	268	–1/4	0.307(1)	0.4178(5)	5.2(2)

TABLE 3c. Atomic positional parameters of lawsonite in space group *Cmcm* at 285, 300, 350, and 400 K

Atom	*T* (K)	*x*	*y*	*z*	U_{iso}*100 (Å²)
Ca	285	–1/4	0.0804(6)	1/4	1.1(1)
	300	–1/4	0.0807 (6)	1/4	1.2(1)
	350	–1/4	0.0805(6)	1/4	1.4(1)
	400	–1/4	0.0803(6)	1/4	1.4(1)
Al	285	0	1/4	0	0.5(1)
	300	0	1/4	0	0.6(1)
	350	0	1/4	0	0.7(1)
	400	0	1/4	0	0.7(1)
Si	285	–1/4	0.7311(4)	0.1330(3)	0.42(8)
	300	–1/4	0. 7311(4)	0.1331(3)	0.45(8)
	350	–1/4	0. 7311(4)	0.1331(3)	0.49(8)
	400	–1/4	0. 7309(4)	0.1330(3)	0.52(8)
O1	285	–1/4	–0.2028(4)	1/4	0.64(9)
	300	–1/4	–0.2030(5)	1/4	0.66(9)
	350	–1/4	–0.2033(5)	1/4	0.71(9)
	400	–1/4	–0.2036(5)	1/4	0.89(9)
O2	285	0.0225(3)	0.1283(2)	0.1166(1)	0.61(4)
	300	0.0226(3)	0.1281(2)	0.1167(1)	0.63(5)
	350	0.0223(3)	0.1290(2)	0.1164(1)	0.74(5)
	400	0.0225(3)	0.1288(2)	0.1165(1)	0.75(5)
O3	285	–1/4	–0.1122(3)	0.0675(2)	0.09(6)
	300	–1/4	–0.1123(3)	0.0675(2)	0.13(6)
	350	–1/4	–0.1125(3)	0.0677(2)	0.20(6)
	400	–1/4	–0.1123(3)	0.0678(2)	0.27(6)
O4	285	–1/4	0.3910(3)	0.0480(2)	1.28(7)
	300	–1/4	0. 3913(3)	0.0482(2)	1.28(8)
	350	–1/4	0. 3915(3)	0.0482(2)	1.42(8)
	400	–1/4	0. 3916(3)	0.0481(2)	1.37(8)
O5	285	–1/4	0.3606(6)	1/4	1.7(1)
	300	–1/4	0. 3602(7)	1/4	1.7(1)
	350	–1/4	0. 3615(7)	1/4	2.1(1)
	400	–1/4	0. 3607(7)	1/4	2.2(1)
Dw	285	–1/4	0.4153(6)	0.1886(3)	5.9(1)
	300	–1/4	0. 4160(6)	0.1886(4)	6.0(1)
	350	–1/4	0. 4160(6)	0.1886(4)	6.2(1)
	400	–1/4	0. 4161(6)	0.1889(4)	6.5(1)
Dd	285	–1/4	0.2890(6)	0.0551(4)	7.3(1)
	300	–1/4	0. 2889(6)	0.0554(4)	7.2(1)
	350	–1/4	0. 2896(6)	0.0556(4)	7.6(1)
	400	–1/4	0. 2893(6)	0.0557(4)	7.5(1)

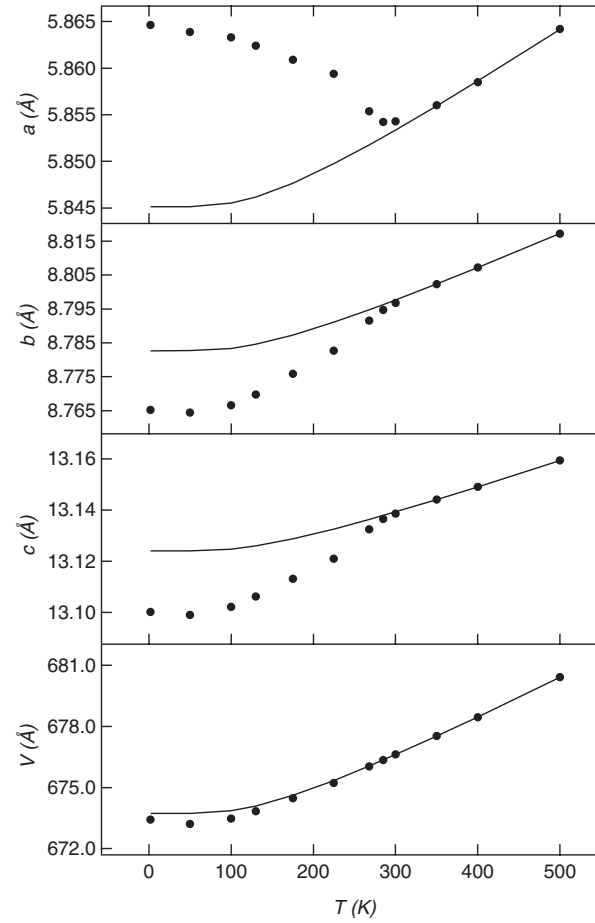

FIGURE 1. Lattice constants of lawsonite between 2 and 500 K from neutron diffraction. The *coth*-function used as a baseline in spontaneous strain calculations is also shown in the figures. Estimated standard deviations are smaller than the symbol size.

direction indicated by the straight line in the 285 K plot in Figure 4. They do not quite cut through the central positions of the D atoms, but they do show the shifts below T_2. Above T_2 Dwa and Dw oscillate in a direction perpendicular to the chain, while the deuterium atoms which form OD bonds oscillate in the plane of the chain. Above T_1 these oscillations become stronger (bottom of the Fig. 6).

A displacive order parameter?

To quantify the shifts in atomic positions with temperature, a quantity δ was calculated as the modulus of the vector difference between atomic positions at two temperatures:

$$\delta = \sqrt{(x_{400} - x_T)^2 + (y_{400} - y_T)^2 + (z_{400} - z_T)^2}\,. \qquad (2)$$

The index 400 refers to the 400 K data set, which was taken as reference state and the index *T* to the data at any temperature. Thus, δ is a measure of the shift of each atom from its average position in the parent *Cmcm* structure. The δ atoms O2 (Fig. 7), Dd and Dda (Fig. 8) and Dw and Dwa (Fig. 9) show the most pronounced effects. The deviation from zero for the O2 atom, δO2, is only small from high temperatures down to 285 K, when it starts to increase smoothly. At ~T_2 it shows a jump and almost doubles its magnitude. $(\delta O2)^4$ is shown in the lower part of Figure 7 and the linear relationship implies that δO2 is scaling linearly with the order parameter for the temperature range between T_1 and T_2. The displacements of other oxygen atoms are all much smaller. The variation of δDd (Fig. 8) has an apparent discontinuity between 268 K and 285 K, but shows no influence by the transition at T_2. The magnitude of δDda is almost twice that of δDd, whereas $(\delta Dd)^4$ and $(\delta Dda)^4$ both vary approximately linearly with temperature (lower part of Fig. 8). The thermal evolution of δDwa (Fig. 9) is quite similar to that of δO2, with a large displacement at T_2, whereas the variation δDw is more like that of δDd and δDda.

O-D, O···D, O-O distances

Figure 10 schematically shows the four different D positions with coordinating oxygen atoms in the $P2_1cn$ structure of lawsonite. Within a cut-off distance of 2.6 Å, four oxygen at-

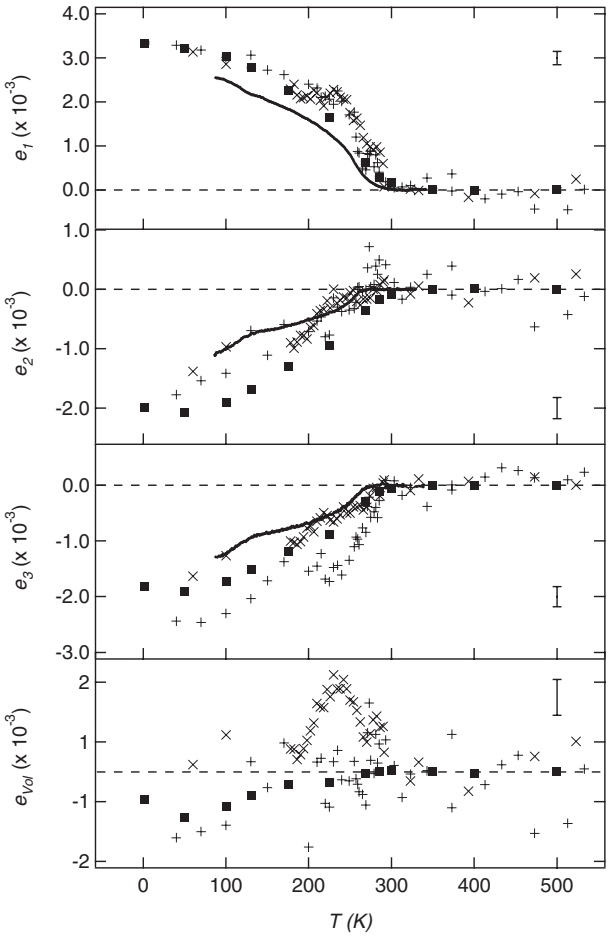

FIGURE 2. Spontaneous strain for lawsonite from neutron diffraction (squares), X-ray diffraction (plus signs and crosses) and dilatometry data (dots). The error bar in each plot is the estimated standard deviation of the X-ray experiments. Estimated standard deviations for the neutron data are smaller than the symbol size.

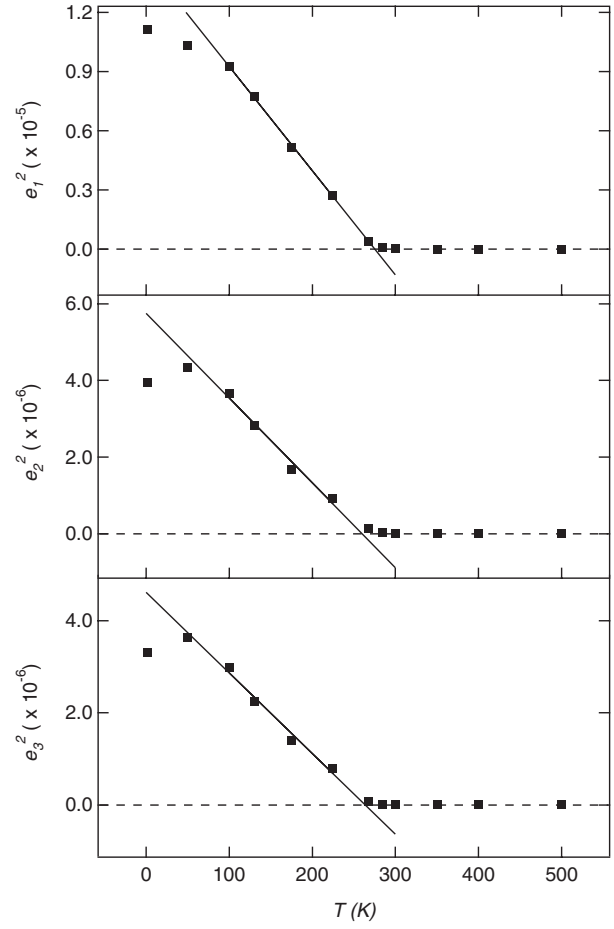

FIGURE 3. Thermal evolution of the square of the spontaneous strains, e_i^2, indicating tricritical behavior below T_1 (=273 K).

oms are nearest neighbors and nine oxygen atoms are next-nearest-neighbors of the deuterium atoms.

Two oxygen atoms coordinate Dw: O5 is at a distance of 1.019(4) Å away and O4 is located 1.586(4) Å away. Both distances are near the ideal bond lengths for hydrogen bonds (Libowitzky 1999). The Dd atom is shown with four oxygen neighbors, the O4 atom having a distance of 1.024(4) Å from Dd. Of the other three oxygen atoms, O4a is at an almost typical distance of 1.662(4) Å, while O2 and O2c occupy positions 2.484(9) Å and 2.398(9) Å, respectively, away from Dd. For Dda four neighboring oxygen atoms are observed; O4a, at a distance of 0.939(4) Å, is the nearest neighbor. The distance to the next-nearest atom (O5) is 2.035(6) Å and the atoms O2a and O2b are observed at comparatively large distances of 2.294(9) and 2.398(9) Å, respectively. Around the Dwa atom, three coordinating oxygen atoms are observed within a distance of 2.6 Å. O5 forms the nearest neighbor at 0.942(5) Å, whereas both the other atoms deviate quite clearly from ideal D-O distances with a separation of 2.217(8) Å and 2.400(5) Å.

Figure 11 and Table 4 show the temperature variations of the D-O distances of Figure 10. Above T_1 the D atoms are constrained by symmetry to two independent positions (Dw and Dd), whereas in the two low temperature space groups each of these splits into two (Dw, Dwa, Dd, Dda). Three of the four short O-D distances (Dw-O5, Dd-O4 and Dda-O4a) seem not to be affected by the symmetry change at T_2, which is in contrast to the behavior of the Dwa-O5 distance (Table 4a).

The remaining nine D-O distances show different temperature dependencies (Table 4b). The Dw-O4 distance at about 1.6 Å increases slowly over a large temperature range and seems to significantly change this behavior on heating only in the vicinity of T_1. A similar temperature dependency is shown by Dd-O4a, but with slightly higher values for the bond length. The other two Dd-O distances, Dd-O2 and Dd-O2c at ~2.4 Å

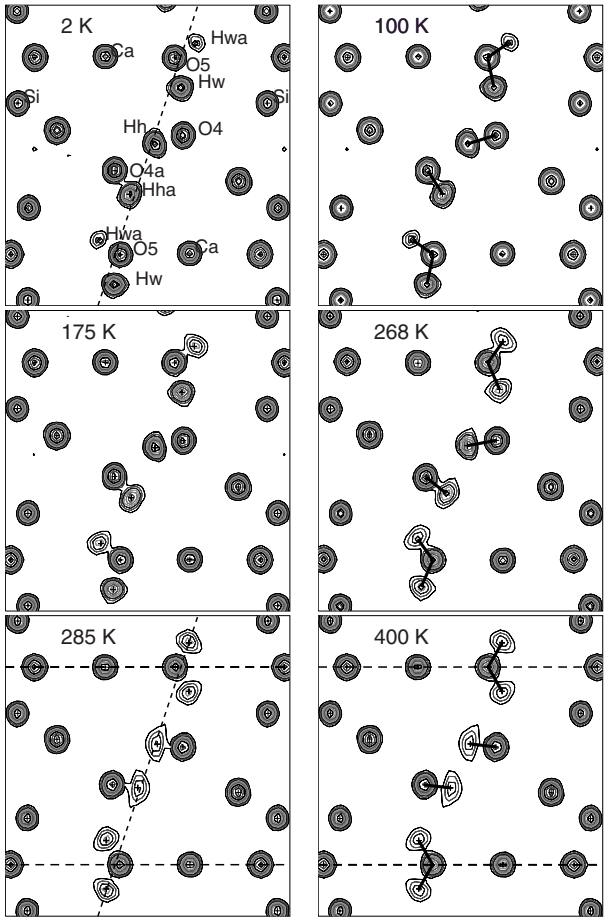

FIGURE 4. Fourier maps (F_{obs}) of the lawsonite structure containing a D_2O-OD-OD-D_2O chain. Dashed lines equal mirror planes in the high symmetry space group. The dashed inclined line in the 2 K and 285 K plots indicates the direction of the second cut through the nuclear density shown in Figure 6. The **c**-axis points upwards, **b** to the right. Contour intervals are 0.5 fm/Å^3 between 0.50 and 6.

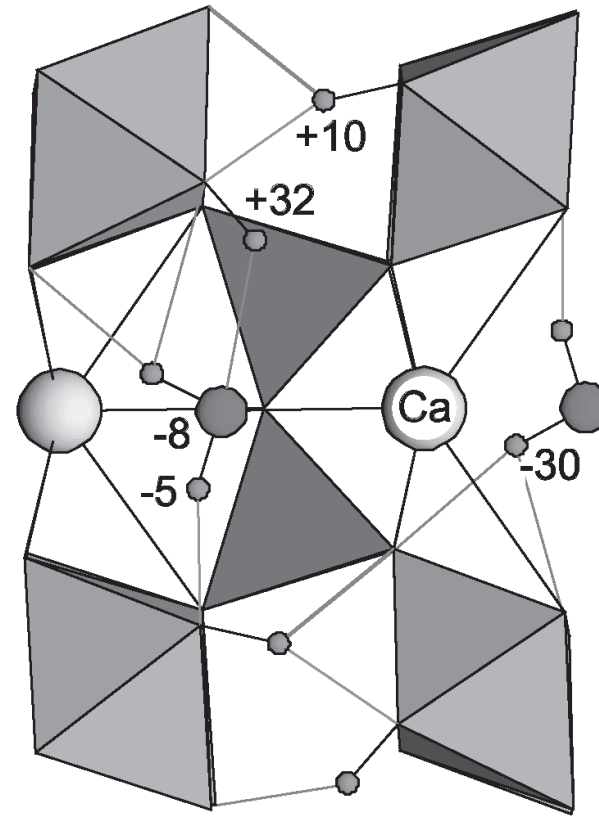

FIGURE 5. Polyhedral drawing of a part of the $P2_1cn$-lawsonite structure in the same orientation as in Figure 4. The arrangement of hydrogen atoms can be followed from two OH at the bottom of the plot via the H_2O molecule to the next two OH molecules (reproduced with kind permission of E. Libowitzky). The numbers refer to the deviation of the atoms from the lost (100) mirror-plane (x=0) in Libowitzky's structure model.

merge above T_2 and subsequently decrease slightly. Dda-O5 is at ~2.0 Å at low temperatures and increases to ~2.2 Å at T_1, where it increases abruptly to 2.6 Å. Two other Dda-O distances below 2.6 Å, between Dda and O2b and O2a, merge above T_2 and exhibit a negligible variation over the temperature range. Dwa-O2 and Dwa-O4a show contrasting behavior to each other. Whereas Dwa-O2 increases in steps from 2.2 to 2.5 Å, Dwa-O4a decreases with temperature.

The O-D···O distances (Fig. 12) were calculated for the D-O environments in Figure 10. They cover a range between 2.6 and 3.2 Å. The two shortest distances (at low temperatures) are O5-Dw···O4 and O4-Dda···O4a. The next longest distance is shown for O4a-Dda···O5 and O5-Dwa···O4a, which plot on top of each other. Above T_1, O5-Dwa···O4a becomes O5-Dw···O4, and is therefore not plotted above this temperature.

Around 2.9 Å, the O4a-Dda···O2a and O4a-Dda···O2b distances merge above T_2. O4-Dd···O2 and O4-Dd···O2c are also separate below T_2 only. They were calculated at 2.95 and 3.1 Å, respectively. The longest separation is the O-O distance O5-Dw···O2 at 3.2 Å.

DISCUSSION

One of our objectives was to determine how far the deuterium-hydrogen exchange affected the critical temperatures and the thermodynamic character of the transitions. Sondergeld et al. (2000); Martin-Olalla et al. (2001); and Meyer et al. (2000) showed that the transition at T_1=273 K in a non-deuterated sample can be described by a tricritical model. From Figure 2, the spontaneous strains of a deuterated sample are qualitatively the same as those of non-deuterated samples. That the deuteration process does not change the thermodynamic character is demonstrated in Figure 3, which shows that the squares of the spontaneous strains, e_i^2, vary linearly with temperature. The transition at T_1 in both deuterated and non-deuterated lawsonite is thus tricritical within experimental uncertainty. The critical temperature of T_1=273 K determined by a linear fit to the data (Fig. 3) is in excellent agreement with the transition tempera-

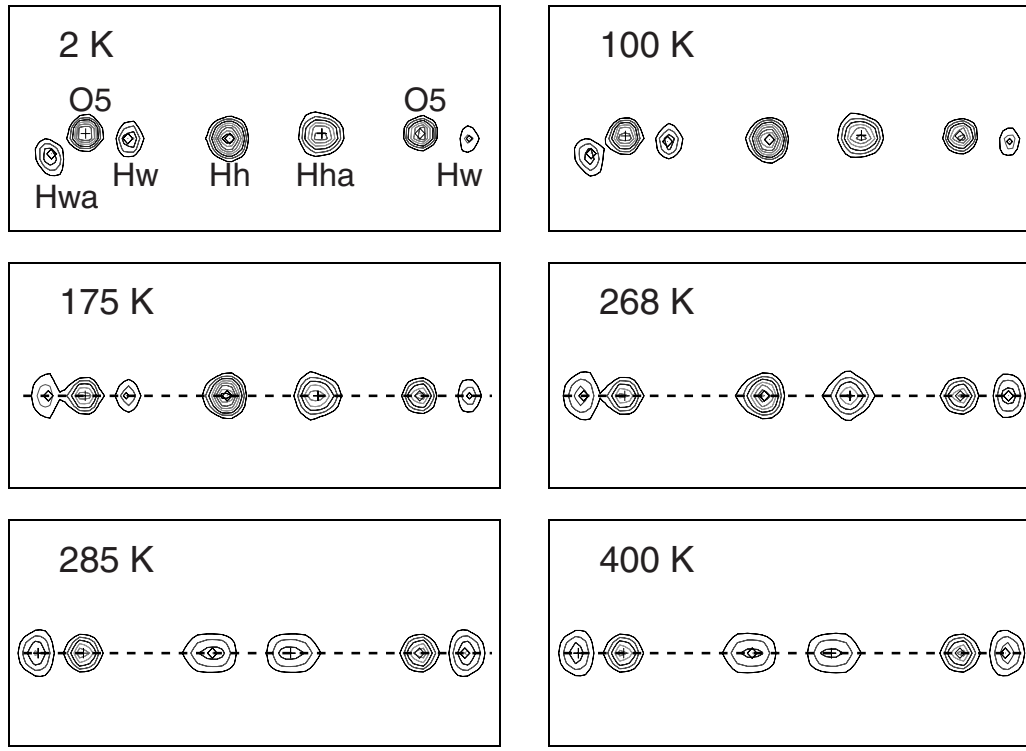

FIGURE 6. The nuclear density maps for the second orientation indicated on Figure 4 by a dashed inclined line. Temperature-induced increases of atomic displacements are shown. The sequence indicates the development of the ferroelectric pattern below the second transition, (the top row).

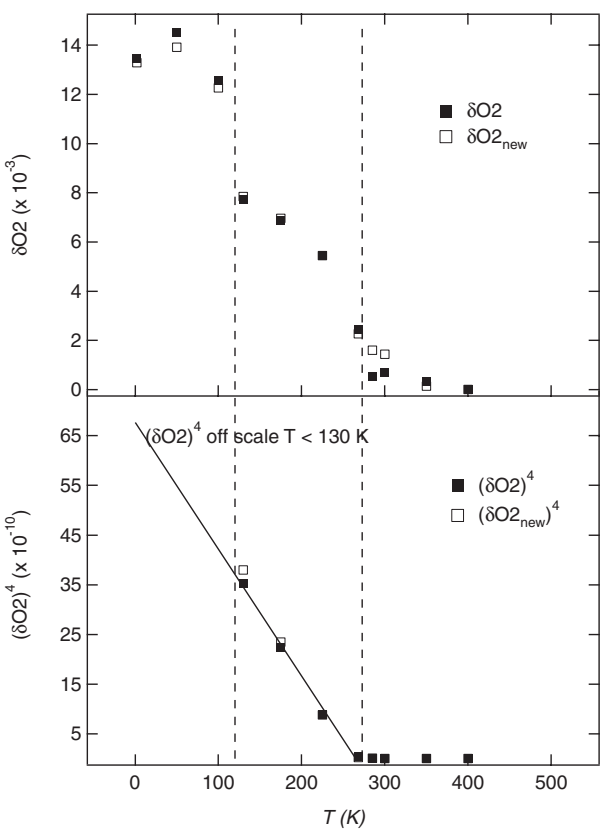

ture determined by specific heat measurements on a non-deuterated sample (Martin-Olalla et al. 2001). Thus, the transition mechanism is not determined by the dynamics of the H or D motions. This contrasts with, for example, TlH_2PO_4 and TlD_2PO_4, in which the transition temperature changes from 230 K to 353 K due to the substitution of D for H (Rios et al. 1998).

For lawsonite the behavior of the spontaneous strain below T_1 can be described with a Landau model, which implies that a description of the phase transition on an atomic scale must involve displacive components as opposed to a model that depends only on the configurational effects of atomic ordering. This issue has been discussed in detail (Carpenter 1992; Carpenter et al. 1994; Martin-Olalla et al. 2001). Shifts of atomic positions of the type shown in Figures 7, 8, 9 can be used to look for such components. δO2, δDw, and δDwa seem to vary continuously at T_1, whereas the thermal evolution of δO2 and δDwa at T_2 changes more abruptly. More abrupt changes exist in δDd and δDda (Fig. 8) at T_1, but the shifts still roughly scale as $\delta^4 \sim (T - T_c)$. These shifts of atomic positions describe the

◀

FIGURE 7. (Top) The atomic shift of the O2 atom for refinements in the highest possible space group for each temperature interval (δO2, full symbol), and in the reduced-symmetry space group (δO2$_{new}$, open symbol). Both show a continuous behavior below T_1 and a discontinuity at T_2. **(Bottom)** $(\delta O2)^4$ (left axis) and $(\delta O2_{new})^4$ (right axis) both display linear temperature dependency below T_1. The line is a guide to the eye.

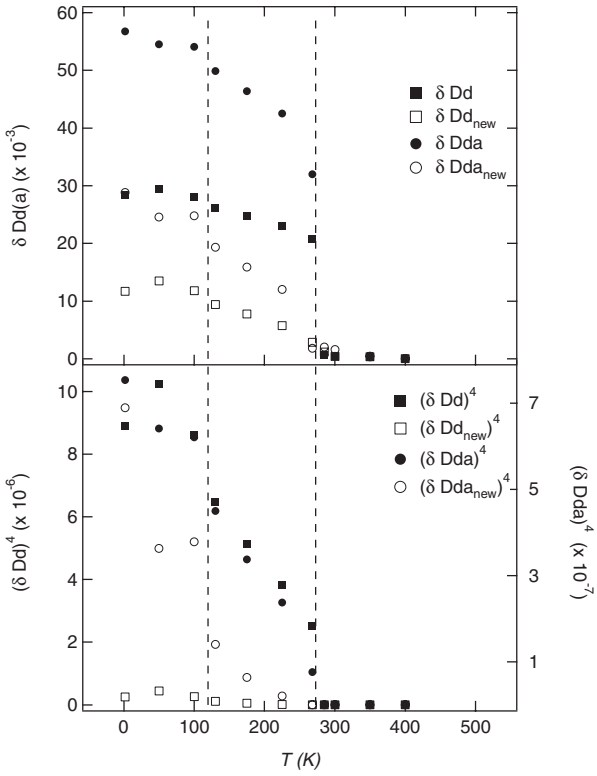

FIGURE 8. Atomic shifts of the Dd deuterium atoms as a function of temperature. (**Top**) The atomic shift of the Dd deuterium atoms as a function of temperature shows a discontinuity at T_1 for both Dd and Dda, but a more continuous temperature dependence as a result of the second refinement process (δDd_{new}, δDda_{new}). (**Bottom**) The behavior of $(\delta Dda)^4$ maybe interpreted as continuous contrast to $(\delta Dd)^4$, which clearly is non-continuous. The changes in $(\delta Dd_{new})^4$ and $(\delta Dda_{new})^4$ are indeed too small for any statement. Left axis: $(\delta Dd)^4$, right axis: all other symbols.

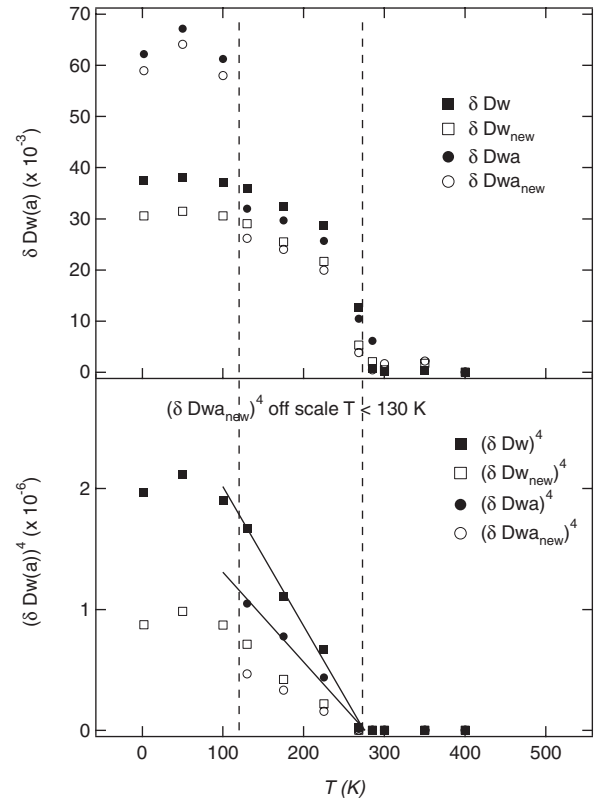

FIGURE 9. (Top) The thermal evolution of the atomic shift of the Dw deuterium atoms gives evidence of continuous changes for the temperature range down to T_2. There the data for Dwa and Dwa_{new} are both highly affected by the transition, Dw and Dw_{new} seem rather unimpressed. **(Bottom)** $(\delta Dw)^4$ and $(\delta Dwa)^4$ both display a temperature dependence close to linear. The lines are drawn in as guides to the eye.

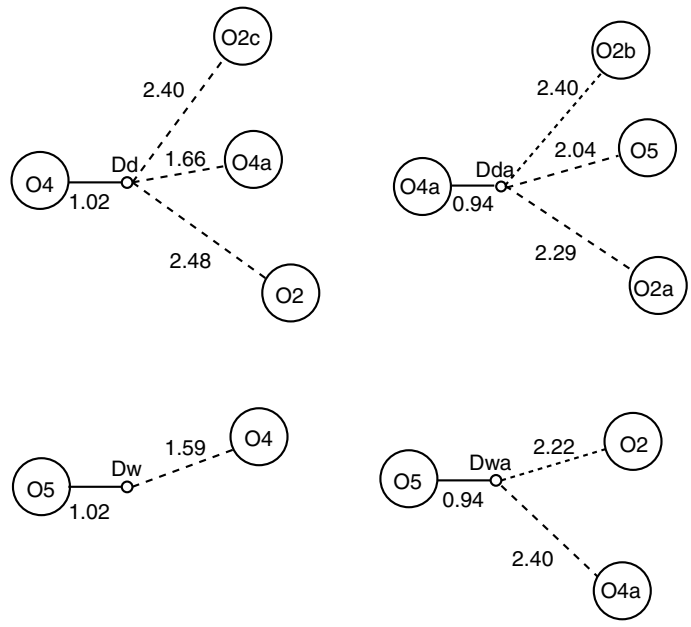

FIGURE 10. Schematic drawing of the deuterium positions and some neighboring oxygen atoms as observed in the $P2_1cn$ structure of lawsonite at 2 K. The cut-off distance for the graph was chosen at 2.6 Å.

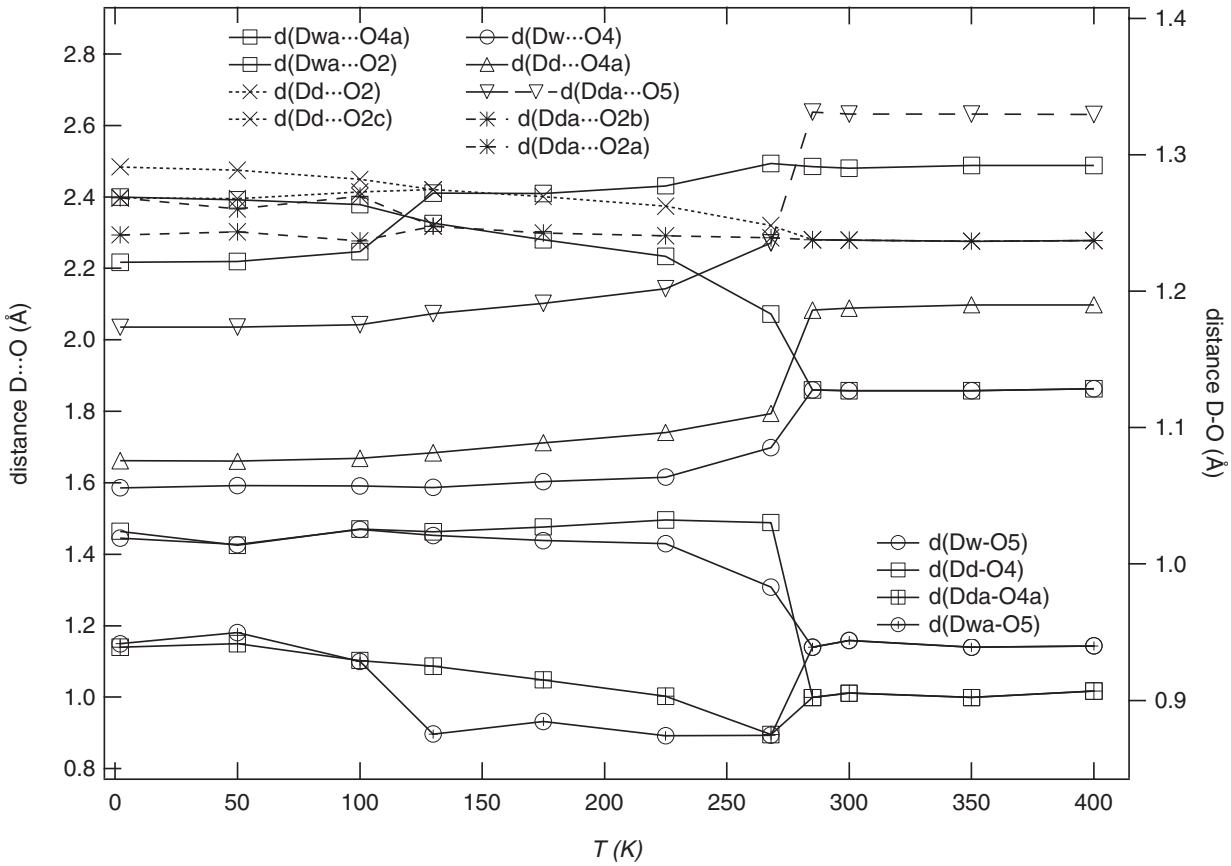

FIGURE 11. D-O distances for the D-O pairs of Figure 10. The right axis pertains to the four O-D distances with a length of ~1 Å at the bottom of the figure. The other bond lengths (left axis) are next-nearest-neighbor distances calculated for the deuterium-oxygen pairs of Figure 10 separated more than 1.6 Å from each other.

TABLE 4a. Thermal evolution of the D-O distances from Figure 11

T (K)	Dw-O5 (Å)	Dwa-O5 (Å)	Dd-O4 (Å)	Dda-O4a (Å)
2	1.019(4)	0.942(5)	1.024(4)	0.939(4)
50	1.018(4)	0.944(5)	1.025(5)	0.930(4)
100	1.025(5)	0.928(5)	1.026(5)	0.929(4)
130	1.021(5)	0.875(5)	1.024(5)	0.925(4)
175	1.017(5)	0.884(5)	1.027(5)	0.915(5)
225	1.014(6)	0.874(6)	1.032(6)	0.903(5)
268	0.983(9)	0.874(9)	1.030(9)	0.875(8)
285	0.939(4)	0.939(4)	0.902(5)	0.902(5)
300	0.944(5)	0.944(5)	0.905(6)	0.905(6)
350	0.939(5)	0.939(5)	0.902(6)	0.902(6)
400	0.940(5)	0.940(5)	0.907(6)	0.907(6)

TABLE 4b. Thermal evolution of the D-O distances from Figure 11

T (K)	Dwa-O4a (Å)	Dw-O4 (Å)	Dd-O4a (Å)	Dd-O2 (Å)
2	2.400(5)	1.586(4)	1.662(4)	2.484(9)
50	2.392(5)	1.592(5)	1.660(5)	2.48(1)
100	2.378(5)	1.591(5)	1.668(5)	2.45(1)
130	2.326(5)	1.587(5)	1.684(5)	2.420(4)
175	2.280(6)	1.603(6)	1.712(6)	2.401(4)
225	2.234(6)	1.616(6)	1.741(6)	2.374(4)
268	2.07(1)	1.70(1)	1.794(8)	2.320(7)
285	1.860(5)	1.860(5)	2.083(6)	2.280(5)
300	1.858(6)	1.858(6)	2.089(6)	2.279(4)
350	1.858(5)	1.858(5)	2.098(6)	2.276(5)
400	1.863(5)	1.863(5)	2.098(6)	2.278(5)

TABLE 4c. Thermal evolution of the D-O distances from Figure 11

T (K)	Dwa-O2 (Å)	Dda-O5 (Å)	Dda-O2a (Å)	Dda-O2b (Å)	Dd-O2c (Å)
2	2.217(8)	2.035(6)	2.294(9)	2.398(9)	2.398(9)
50	2.219(9)	2.036(7)	2.30(1)	2.39(1)	2.40(1)
100	2.25(1)	2.042(7)	2.28(1)	2.40(1)	2.41(1)
130	2.411(5)	2.073(7)	2.318(4)	2.318(4)	2.420(4)
175	2.410(6)	2.102(8)	2.299(5)	2.299(5)	2.401(4)
225	2.431(6)	2.143(9)	2.291(5)	2.291(5)	2.374(4)
268	2.49(1)	2.27(2)	2.286(9)	2.286(9)	2.320(7)
285	2.485(5)	2.637(6)	2.280(5)	2.280(5)	2.280(5)
300	2.480(5)	2.632(6)	2.279(4)	2.279(4)	2.279(4)
350	2.488(5)	2.632(6)	2.276(5)	2.276(5)	2.276(5)
400	2.488(6)	2.631(6)	2.278(5)	2.278(5)	2.278(5)

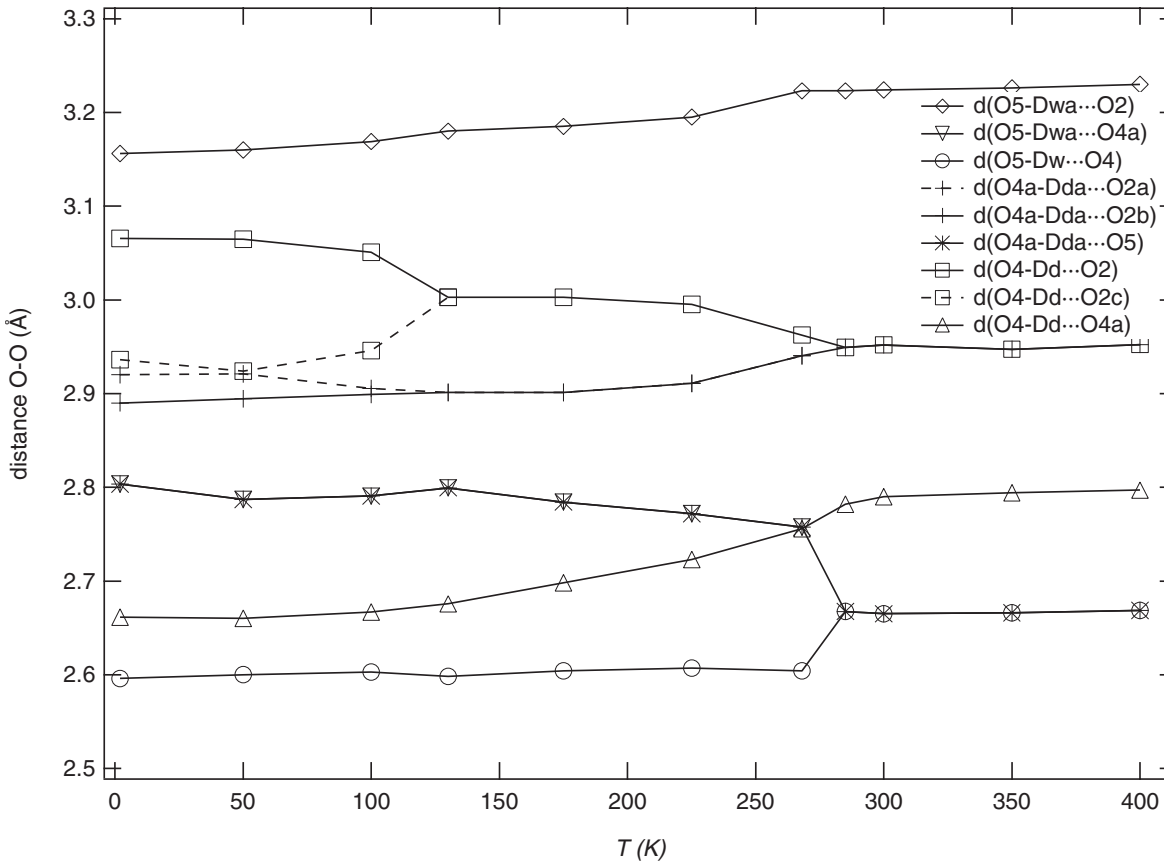

FIGURE 12. O-D···O distances vs. temperature, calculated from O···O pairs from Figure 11. The O5-Dwa···Ox bonds do not correlate to the temperature dependence of the relevant IR mode.

average structure only, however, and do not discriminate between displacive and order-disorder models. This is because the average positions of atoms partially disordered between split sites can appear to be somewhere in between the actual sites. The data above T_1 were also refined in space group *Pmcn* to test whether the sites in the *Cmcm* structure might be split. In the range between T_1 and T_2 it was unsuccessfully attempted to refine the structures in space group $P2_1cn$. The results of these refinements in *Pmcn* (Figs. 7 to 9) essentially confirm the previous findings for O2, Dw and Dwa. The choice of refinement procedure does affect whether or not a discontinuity for Dd and Dda is observed. These refinements may not elucidate the transition mechanism but they do confirm that the framework participates significantly in the phase transitions. It is also possible that the changes in atomic positions at T_2 are more abrupt than those at T_1, but this remains a highly tentative conclusion. From their infrared study, Libowitzky and Rossman (1996) concluded that the protons in the *Cmcm* structure are dynamically disordered between split positions and then order at the phase transitions. An equivalent method for investigating local structural behavior is needed to test whether the O2 atoms, in particular, of the framework behave in the same way.

The new structural data can be used to check details of the assignments given by Libowitzky and Rossman (1996) for the four O-H stretching modes observed in infrared spectra in the range ~2800–3600 cm^{-1} by comparing the O-H frequencies with D-O and O···O distances. In Figure 13 data for the four O-H stretching modes are reproduced from Meyer et al. (2000) at ~2800 cm^{-1} (bottom), 3200 cm^{-1} (center), 3550 and 3620 cm^{-1} (top). At temperatures above 260 K the high frequency peaks become indistinguishable. Frequencies for three of these peaks (at 2800, 3200, and 3550 cm^{-1}) increase with increasing temperature, whereas the fourth peak at 3620 cm^{-1} shows the opposite trend. As reviewed by Libowitzky (1999), O-H stretching frequencies correlate with O···H and O···O distances. The D-O, D···O and O···O distances are again only for the average structure but they are much greater than the shifts of the atomic positions, δ, and are not significantly affected by considerations of the average versus split positions of the D atoms.

First, there is an approximate correlation between the O-H stretching frequency and the O-D distances in that a short O-D distance corresponds with a high O-H frequency, and vice versa. Below T_1 the O-D distances (Fig. 11) are grouped in two pairs while the O-H frequencies are spread into four discrete ranges (Fig. 13), however, which suggests that other factors must also

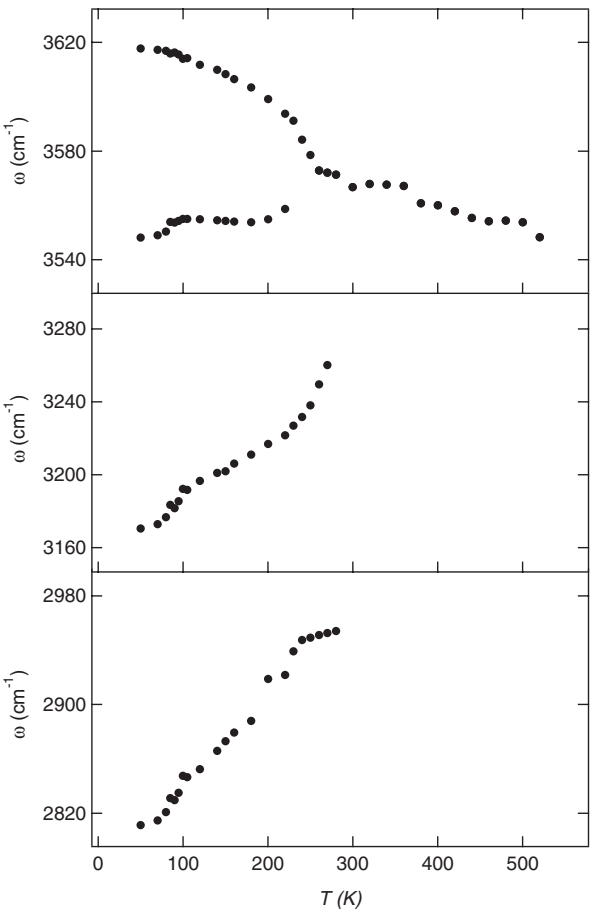

FIGURE 13. Temperature dependence of the peak positions of the four OH stretching modes in lawsonite as observed in IR experiments (Meyer et al. 2000). The two low frequency peaks at ~2800 cm^{-1} and 3200 cm^{-1} could not be detected above 290 K and 270 K, respectively.

influence the stretching frequencies. The mode with the lowest frequency is at ~2838 cm^{-1}, therefore this must correlate to the shortest D···O distance shown on the graph. This is the Dw···O4 hydrogen bond (1.6 Å at 2 K). The corresponding O5···O4 distance in O5-Dw···O4 of 2.603 Å (Fig. 12) is also close to the ideal distance of 2.5 Å observed in hydrogen bonds. The second shortest D-O distance of 1.67 Å, between atoms Dd and O4a, is assigned to the stretching mode with the next-highest frequency at 3200 cm^{-1}. The corresponding distance between O4 and O4a in O4-Dd···O4a is 2.66 Å, as shown in Figure 12. For both these modes, increasing the D···O length correlates with increasing frequency for O-H stretching.

The remaining two O-H stretching frequencies are observed at ~3550 cm^{-1} and ~3620 cm^{-1} at low temperatures. The separation between the two modes is small at low temperatures, whereas at higher temperatures the two modes become indistinguishable. Libowitzky and Rossman (1996) assigned these to O4a-Hha and O5-Hha. The Dda···O5 bond in O4a-Dda···O5 has a bond length of 2.03 Å at 2 K and increases to ~2.2 Å at T_2. Again, the increasing D···O distances correlates with increasing O-H stretching frequency

The remaining mode at 3620 cm^{-1} is assigned to O5-Hwa stretching and the corresponding D···O distance in O5-Dwa···O2 is 2.21 Å at 2 K. There is also a D···O distance of 2.4 Å at 2 K in O5-Dwa···O4a, however. With increasing temperature these two D···O distances change in such a way that at $T > T_2$ the Dwa···O4a distance is smaller than the Dwa···O2 distance. In other words the hydrogen-bonding configuration changes at the $Pmcn \leftrightarrow P2_1cn$ transition point. The trend of decreasing D···O distance with increasing temperature then correlates with the trend of decreasing O-H stretching frequency.

In Figure 14 the frequencies of the O-H stretching modes are plotted versus the four next-nearest neighbor D···O distances, as discussed above. The function derived by Libowitzky (1999) from data for many minerals

$$\nu(cm^{-1}) = 3632 - 1.79 \times 10^{6}*\exp[-d(H\cdots O)/0.2146\ (cm^{-1})] \quad (3)$$

is shown for comparison. The overall agreement between distances and frequencies is consistent with these detailed assignments, allowing that O-D stretching frequencies are systematically lower than O-H stretching frequencies. The high frequency stretching mode data for 300 K and above, plot significantly off the expected trend and reinforce the conclusion of Libowitzky and Rossman (1996) that the protons are disordered between discrete sites in the *Cmcm* structure rather than being located at their high symmetry positions. Libowitzky (1999) also found an equivalent correlation between O···O distances and O-H frequencies, but this is not observed for the O···O distances found here. This presumably reflects the relatively complex distribution of oxygens around the Dwa and Dda atoms in lawsonite.

Whereas the mechanism for the $Cmcm \leftrightarrow Pmcn$ transition

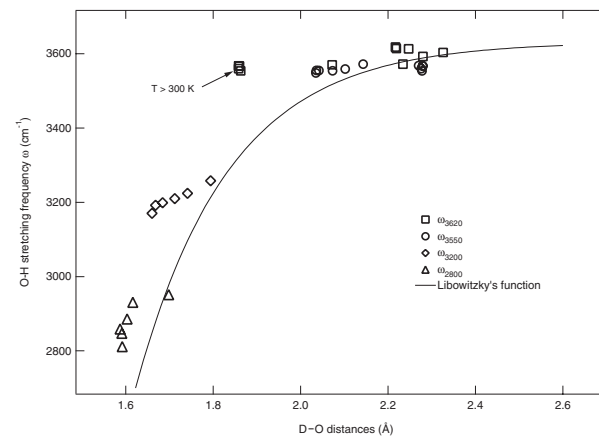

FIGURE 14. Correlation of O-H stretching frequencies from Figure 13 with observed O···D bonds. Also shown is a function predicting the frequency-distance relationship as derived by Libowitzky (1999). In general, the agreement between the data pairs observed frequency/D-O bond is good for low temperature data. The arrow indicates data points of the high frequency stretching mode above ~300 K which plot significantly away from the general trend.

in lawsonite can be understood in terms of proton ordering, there is also a significant contribution from framework displacements. The same may also be true of the $Pmcn \leftrightarrow P2_1cn$ transition but the thermodynamic character of this transition has not been so well defined.

ACKNOWLEDGMENTS

We thank C. Francis from Harvard University, USA, for supplying the sample used in this study. Thanks also go to B.C. Schmidt (Bayreuth, Germany) for carrying out the NMR experiments and to Rutherford Appleton Laboratory for providing beam time at ISIS. This work was performed within and financially supported by the European Union TMR-Network on Mineral Transformations (contract no. ERB-FMRX-CT-97-0108).

REFERENCES CITED

Carpenter, M.A. (1992) Thermodynamics of phase transitions in minerals: A macroscopic approach. In G.D. Price & N.L. Ross, eds., In The stability of minerals, 172–215 p. Chapman and Hall, London.

Carpenter, M.A., Powell, R., and Salje, E.K.H. (1994) Thermodynamics of nonconvergent ordering in minerals: I. An alternative approach. American Mineralogist, 79, 1053–1067.

Carpenter, M.A., Salje, E.K.H., and Graeme-Barber, A. (1998) Spontaneous strain as a determinant of thermodynamic properties for phase transitions in minerals. European Journal of Mineralogy, 10, 621–691.

Ibberson, R.M., David, W.I.F., and Knight, K.S. (1992) The high resolution powder diffractometer (HRPD) at ISIS – a user guide. Rutherford Appleton Laboratory Report RAL-92–031.

Johnson, M.W. and David, W.I.F. (1985) HRPD: The high resolution powder diffractometer at the SNS. Rutherford Appleton Laboratory Report RAL-85–112.

Lager, G.A., Libowitzky, E., and Schultz, A.J. (1999) Neutron diffraction study of the low-temperature phase transitions in lawsonite. Proceedings of the 17th General Meeting of the International Mineralogical Association, Toronto, A99.

Larson, A.C. and Von Dreele, R.B. (1994) General Structure AnalysisSystem (GSAS), Los AlamosLaboratory Report LAUR 86-748.

Libowitzky, E. (1999) Correlation of O-H stretching frequencies and O-H···O hydrogen bond lengths in minerals. Monatshefte für Chemie, 130, 1047–1059.

Libowitzky, E. and Armbruster, T. (1995) Low-temperature phase transitions and the role of hydrogen in lawsonite. American Mineralogist, 80, 1277–1285.

Libowitzky, E. and Rossman, G. R. (1996) FTIR spectroscopy of lawsonite between 82 and 325 K. American Mineralogist, 81, 1080–1091.

Martin-Olalla, J.–M., Hayward, S.A., Meyer, H.-W., Ramos, S., del Cerro, J., and Carpenter, M.A. (2001) Phase transitions in lawsonite: a calorimetric study. European Journal of Mineralogy, in press.

Meyer, H.–W., Carpenter, M.A., Graeme-Barber, A., Sondergeld, P., and Schranz, W. (2000) Local and macroscopic order parameter variations associated with low temperature phase transitions in lawsonite, $CaAl_2Si_2O_7(OH)_2 \cdot H_2O$. European Journal of Mineralogy, 12, 1139–1150.

Pawley, A.R. (1994) The pressure and temperature stability limits of lawsonite: implications for H_2O recycling in subduction zones. Contributions to Mineralogy and Petrology, 118, 99–108.

Pawley, A.R., Redfern, S.A.T., and Holland, T.J.B. (1996) Volume behavior of hydrous minerals at high pressures and temperatures: I. Thermal expansion of lawsonite, zoisite, clinozoisite, and diaspore. American Mineralogist, 81, 335–340.

Rios, S., Paulus, W., Cousson, A., Quilichini, M., and Heger, G. (1998) Isotope effect in TlH_2PO_4 and TlD_2PO_4. Acta Crystallographica, B54, 790–797.

Salje, E.K.H., Wruck, B., and Marais, S. (1991a) Order parameter saturation at low temperatures – numerical results for displacive and o/d systems. Ferroelectrics, 124, 185–188.

Salje, E.K.H., Wruck, B., and Thomas, H (1991b) Order-parameter saturation and low-temperature extension of Landau theory. Zeitschrift für Physik B, 82, 399–404.

Schmidt, M.W. (1995) Lawsonite: Upper pressure stability and formation of higher density hydrous phases. American Mineralogist, 80, 1286–1292.

Sondergeld, P., Schranz, W., Tröster, A. Carpenter, M.A., Libowitzky, E., and Kityk, A. V. (2000) Optical, elastic and dielectric studies of the phase transitions in lawsonite. Physical Review B, 62, 6143–6147.

MANUSCRIPT RECEIVED AUGUST 2, 2000
MANUSCRIPT ACCEPTED NOVEMBER 28, 2000
MANUSCRIPT HANDLED BY BRYAN CHAKOUMAKOS